

# Losses in Dielectric Image Lines\*

D. D. KING† AND S. P. SCHLESINGER‡

**Summary**—The dipole mode in a dielectric rod permits an image system in which half the dielectric and its surrounding field are replaced by a metal sheet. If the field is allowed to extend many wavelengths outside the rod, the resulting line has very low losses. The contribution of the image surface to line loss is calculated, and shown to be generally less than the dielectric loss. Radiation from obstacles along the line is also discussed. Such obstacles in closed single-mode waveguides are useful for matching purposes. Although matching elements are easily constructed for the image line, radiation loss proves difficult to control.

## INTRODUCTION

LOW ATTENUATION and freedom from higher modes are the principal advantages of the thin dielectric waveguide operated in the  $HE_{11}$  or dipole mode. However, supports and bends are difficult to achieve in the open waveguide. An image system which takes advantage of the plane of symmetry in the  $HE_{11}$  mode removes the support problem and facilitates the design of bends. The properties of bends and various circuit elements in dielectric image line have been discussed in earlier papers.<sup>1,2</sup> In the work to be described, losses in the image line are investigated.

In general, three types of dissipation contribute to the over-all loss in the dielectric image line. They are dielectric loss, conduction loss on the image surface, and radiation. The first of these, dielectric loss, has been calculated for circular rods by Elsasser.<sup>3</sup> We shall extend his formulation of the problem to include the calculation of ohmic loss on the image surface. Experimental results on the various kinds of loss are given, including radiation caused by obstacles along the line.

## CALCULATION OF LOSSES

The field components of the  $HE_{11}$  mode in a circular rod of radius  $a$  can be derived from the longitudinal components by differentiation. These are, inside the rod,

$$\begin{aligned} E_z &= AJ_1(p\rho/a) \cos \phi \\ H_z &= BJ_1(p\rho/a) \sin \phi \end{aligned} \quad (1)$$

and outside the rod,

$$\begin{aligned} E_z &= CK_1(q\rho/a) \cos \phi \\ H_z &= DK_1(q\rho/a) \sin \phi. \end{aligned} \quad (2)$$

\* Manuscript received by the PGM TT, May 5, 1956. Supported by AF Cambridge Res. Ctr., Air Res. and Dev. Command.

† Electronic Communications Inc.; formerly with Johns Hopkins Univ., Baltimore, Md.

‡ Columbia Univ., New York, N. Y.; formerly with Johns Hopkins Univ., Baltimore, Md.

<sup>1</sup> D. D. King, "Properties of dielectric image lines," IRE TRANS., vol. MTT-3, pp. 75-81; March, 1955.

<sup>2</sup> D. D. King, "Circuit components in dielectric image lines," IRE TRANS., pp. 35-39; December, 1955.

<sup>3</sup> W. M. Elsasser, "Attenuation in a dielectric circular rod," *J. Appl. Phys.*, vol. 20, pp. 1192; December, 1949.

Here the common factor  $e^{-i\delta z+i\omega s}$  has been omitted. The parameters  $p$  and  $q$  are related to the propagation constant  $\delta$  by the following relations

$$\begin{aligned} \delta^2 + (p/a)^2 &= \omega^2 \mu_1 \epsilon_1 \\ \delta^2 - (q/a)^2 &= \omega^2 \mu_2 \epsilon_2. \end{aligned} \quad (3)$$

The subscript 1 refers to the constants of the rod, 2 to the space outside the rod. Since only changes in dielectric constants are involved, it is convenient to write

$$\mu_1 = \mu_2$$

$$\epsilon = \epsilon_1/\epsilon_2 = \text{relative dielectric constant of the rod.}$$

Application of the boundary conditions yields a secular equation giving allowed values of  $p$  and  $q$  associated with a particular diameter-to-wavelength ratio for the dielectric rod,  $2a/\lambda_0$ . This parameter is given by

$$\frac{2a}{\lambda_0} = \frac{1}{\pi} \left( \frac{p^2 + q^2}{\epsilon - 1} \right)^{1/2}.$$

The secular equation is

$$(ef + g)(f + g) - (\epsilon/p^2 + 1/q^2)(1/p^2 + 1/q^2) = 0 \quad (4)$$

where the relative permeability  $\mu$  is taken as unity and

$$f = \frac{J_1'(p)}{p J_1(p)} \quad g = \frac{K_1'(q)}{q K_1(q)}.$$

To calculate the attenuation  $\alpha$ , we must find the quantity

$$\left| \frac{1}{\Phi} \frac{d\Phi}{dz} \right| = 2\alpha \quad (5)$$

where  $\Phi$  is the total power flow along the line.

$$\Phi = \int S_z dA$$

$$S_z = E_\rho H_\phi^* - E_\phi H_\rho^*.$$

For dielectric loss in a dielectric rod of conductivity  $\sigma$  we have

$$\frac{d\Phi}{dz} = -\sigma \int_V E^2 dV.$$

We therefore obtain the following final form

$$\left| \frac{1}{\Phi} \frac{d\Phi}{dz} \right| = \frac{2\pi\sigma \int_0^a (E_\rho E_\rho^* + E_\phi E_\phi^* + E_z E_z^*) \rho d\rho}{2\pi \left| \int_0^a S_z \rho d\rho + \int_a^\infty S_z \rho d\rho \right|}. \quad (6)$$

The expression for attenuation obtained by Elsasser is

$$\begin{aligned}\alpha_d &= \frac{1}{2}\sigma\eta \text{ nepers/m} & (\eta &= \sqrt{\mu_0/\epsilon_0}) \\ &= 25.3(\epsilon\phi_0/\lambda_0)R \text{ db/m} & (\phi_0 &= \sigma/\omega\epsilon_1).\end{aligned}\quad (7)$$

The ratio factor  $R$  is a complicated function which we display in the appendix together with a similar factor for the image surface loss.

The loss on the conducting surface of resistance  $R_s = \sqrt{\omega\mu/2\sigma}$  is given by

$$\frac{d\Phi}{dz} = 2R_s \left| \int_0^a (H_\rho H_\rho^* + H_z H_z^*) d\rho + \int_a^\infty (H_\rho H_\rho^* + H_z H_z^*) d\rho \right|_{\phi=\pi/2}. \quad (8)$$

This gives for the attenuation

$$\frac{1}{\Phi} \frac{d\Phi}{dz} = \frac{2R_s \left| \int_0^a (H_\rho H_\rho^* + H_z H_z^*) d\rho + \int_a^\infty (H_\rho H_\rho^* + H_z H_z^*) d\rho \right|_{\phi=\pi/2}}{\pi \left| \int_0^a S_z \rho d\rho + \int_a^\infty S_z \rho d\rho \right|}. \quad (9)$$

The evaluation of this expression is only slightly more difficult than that of (6), which was done by Elsasser.

The resulting expression for  $\alpha_c$  is

$$\begin{aligned}\alpha_c &= (8R_s/\eta\lambda_0)R' \text{ nepers/m} \\ \alpha_c &= (69.5R_s/\eta\lambda_0)R' \text{ db/m}.\end{aligned}\quad (10)$$

The two ratio factors  $R$  and  $R'$  are displayed in the Appendix, together with the definitions of the quantities involved.

#### COMPARISON OF DIELECTRIC AND IMAGE LOSSES

Curves of the attenuation constants  $\alpha_d$  and  $\alpha_c$  are shown in Fig. 1 (opposite). These curves show that the image attenuation  $\alpha_c$  is generally less than the dielectric attenuation in polystyrene. This is true except when the wave is very loosely bound and the dielectric loss becomes extremely small. Even a nichrome image surface fails to raise  $\alpha_c$  to the level of dielectric attenuation  $\alpha_d$  over an appreciable range of  $2\alpha/\lambda_0$ .

Measured points are shown on the curves for both dural and nichrome surfaces. The total attenuation  $\alpha = \alpha_c + \alpha_d$  was measured, and a calculated value of  $\alpha_d$  inserted to obtain  $\alpha_c$ . The loss tangent for polystyrene is usually taken as 0.001; this value was used by Chandler<sup>4</sup> and yielded excellent agreement for  $\alpha_d$ . Since the rod used in the present work was milled flat under oil, and glued to the surface with vinylite cement, some slight increase in the loss tangent might occur. The value 0.002 gives exact agreement between measured and predicted values as shown on the curve. The curve of  $\alpha_d$  shown is based on a compromise value of 0.0015 for the loss tangent.

<sup>4</sup> C. H. Chandler, "An investigation of dielectric rod as wave guide," *J. Appl. Phys.*, vol. 20, pp. 1188-1192; December, 1949.

The resonator with nichrome image surface in place is shown in Fig. 2. A transmission measurement was made to obtain the resonance curve, and hence the loaded  $Q$ . The end losses were separated out by varying the resonator length through a number of resonances. The resulting data are shown in Fig. 3.

The slope of the  $L/Q$  vs length curves yields the line  $Q = \beta/2\alpha$ , and thence the total attenuation  $\alpha$ . Even with

the nichrome image surface,  $\beta/2\alpha = 4000$ . The over-all  $Q$  measured for the full length resonator was about 3000 for nichrome and 5400 for dural image surfaces. A rod with a smaller diameter than 5/16 inch yields a higher  $Q$ , but the 24-inch image surface is too narrow to prevent significant leakage at the edges; this results in unstable operation due to stray coupling.

#### RADIATION LOSS

In the absence of artificial boundaries to the field, there is no radiation loss, *i.e.*, the radial component of the Poynting flux is purely imaginary. On the other hand, the launching elements, bends or obstacles as well as a finite image surface, provide boundaries at which radiation occurs. The case of obstacles suitable for matching purposes is of particular interest, and we shall confine our discussion to such matching elements.

In hollow waveguides, an obstacle which sets up a reflected wave in the dominant mode also produces higher modes which provide reactive energy storage. This process is accompanied only by conduction loss, since the system is enclosed. In the open dielectric line, discontinuities in the line provide reflection in the dominant mode, but the higher modes excited at the obstacle radiate.

To investigate this effect, a number of obstacles have been measured on the interferometer bridge.<sup>2</sup> For unit incident power, the reflected power  $\rho^2$  and the transmitted power  $\tau^2$  were measured simultaneously by the bridge circuit shown in Fig. 4. The results for an iris of 0.035-inch aluminum are plotted in Figs. 5 and 6 (p. 34). Here we note that the radiated power

$$\gamma^2 = 1 - \rho^2 - \tau^2$$

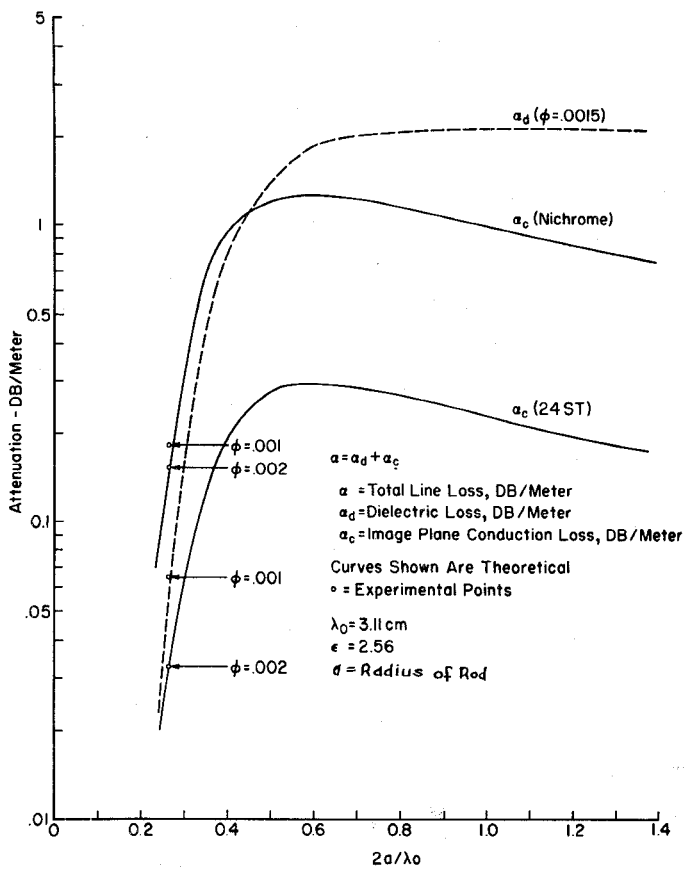


Fig. 1—Calculated attenuation curves for  $\alpha_d$ , polystyrene dielectric, and  $\alpha_c$ , a dural or nichrome image surface. Experimental points for the two image surfaces are shown for two assumed values of dielectric loss tangent  $\phi$ .

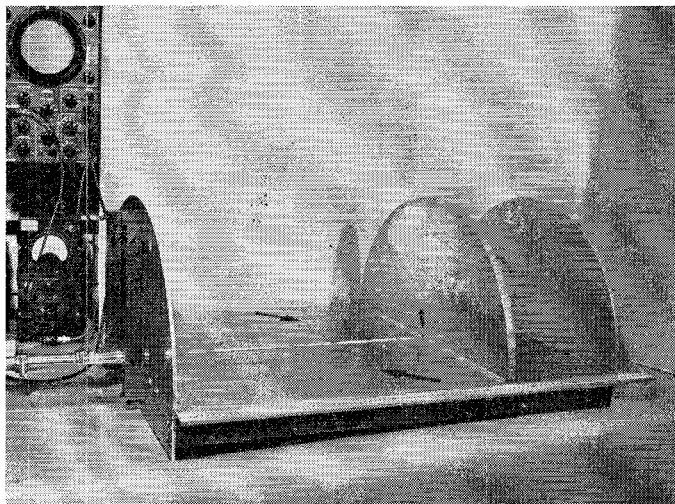


Fig. 2—Resonator for loss measurements at 9636 mc. Large arrows show the nichrome sheet glued to the aluminum surface. Small arrow shows field probe.

is small for both small and large reflections, but becomes large at intermediate ranges. For small apertures the reflecting surface is very sensitive to alignment, as might be expected. A slight backward tilt immediately

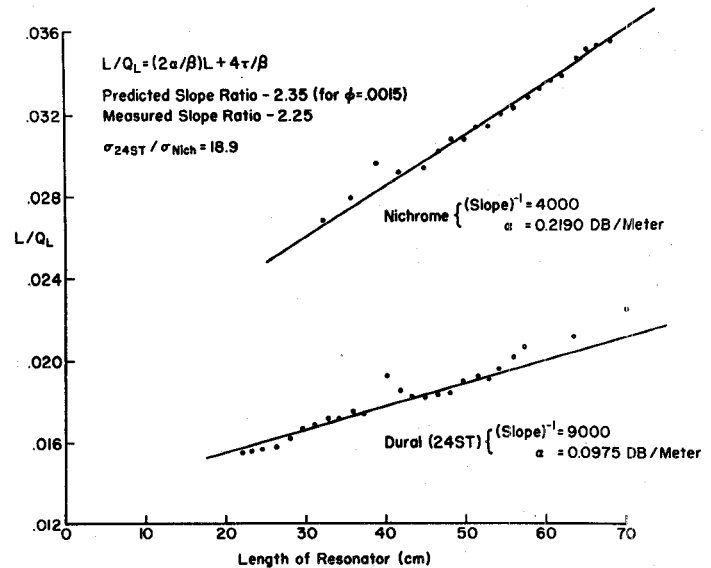


Fig. 3—Plot for separating line loss ( $2\alpha/\beta$ ) from end-face loss ( $\beta/4\tau$ ).

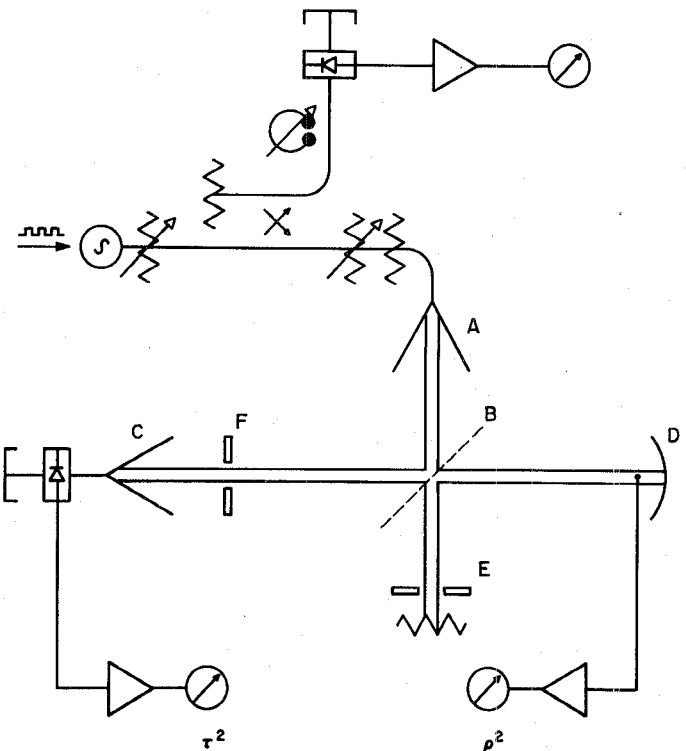


Fig. 4—Interferometer bridge—A) launching horn, B) half-reflecting mirror, C) receiving horn, D) parabolic reflector and coaxial detector, E) matched load, F) obstacle under test.

reduces the reflections along the line and proportionately increases the radiation loss.

A plot of radiation loss  $\gamma^2$  as a function of reflection coefficient  $\rho^2$  for several obstacles is shown in Fig. 7. These include the iris,  $\frac{1}{4} \times \frac{1}{8}$ -inch strips, thin pins, and a dielectric sheet. A photograph of some of these obstacles placed along the line appears in Fig. 8. In general, the radiation loss is least for obstacles acting

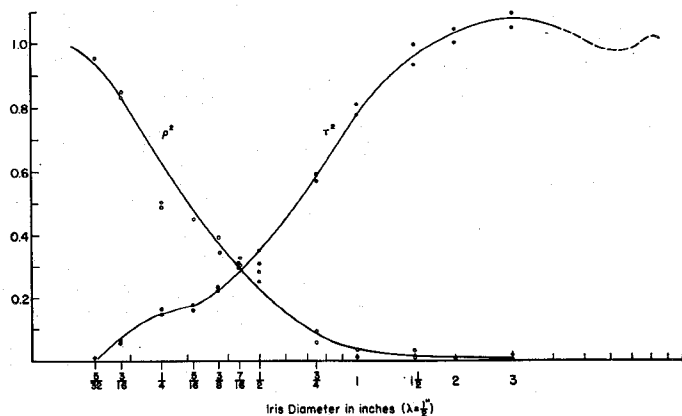


Fig. 5—Reflected power  $\rho^2$  and transmitted power  $\tau^2$  for unit incident power on an iris.

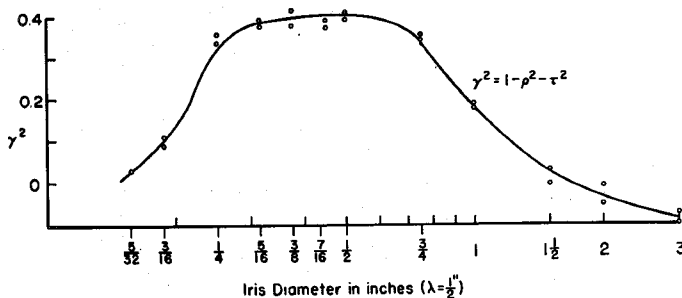


Fig. 6—Radiated power  $\gamma^2$  for unit incident power on an iris.

in regions of high field close to the dielectric. An obstacle presenting only a flat surface across the entire guide produces no radiation, as might be expected by symmetry. Failing this, action on the field near or in the dielectric is most efficient in minimizing radiation loss. Detaching the field from the dielectric altogether is easy to do without reflections. A thin foil cover a few inches long performs this function admirably (see top of Fig. 7).

#### CONCLUSION

Both theory and experiment confirm the fact that an adequate image surface does not significantly alter the attenuation of the  $HE_{11}$  mode. The image loss is generally smaller than the dielectric loss, and decreases in the same rapid manner with the ratio  $2a/\lambda_0$ . This permits extremely low over-all attenuation on image lines with a large cross section in terms of wavelength. Since even a nichrome surface can be operated without objectionable losses, the type of image surface is not critical, even at very short wavelengths. A fine polish, such as is desirable in hollow guide for millimeter operation, is not required on the large image surface which carries low current densities.

The reflection data presented indicate that conventional matching elements produce appreciable radiation loss on an image line. A flat dielectric sheet having the

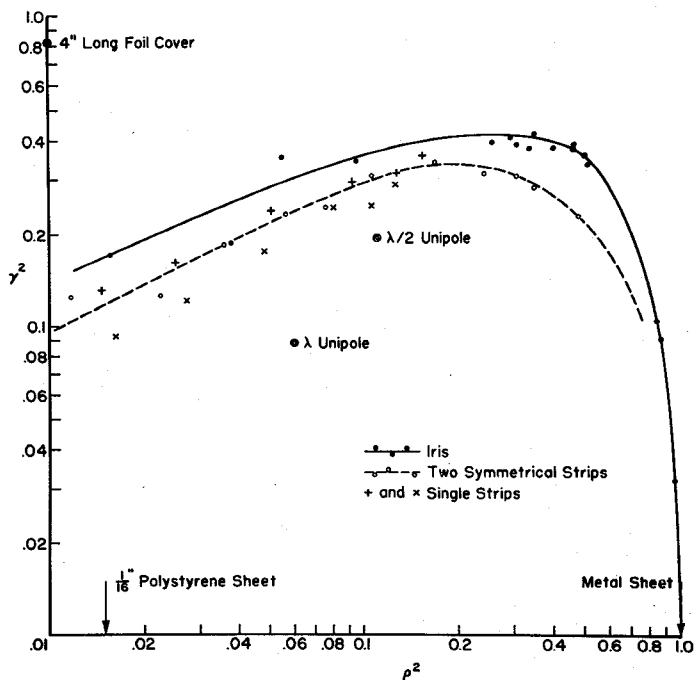


Fig. 7—Radiated power  $\gamma^2$  as a function of reflected power  $\rho^2$ .

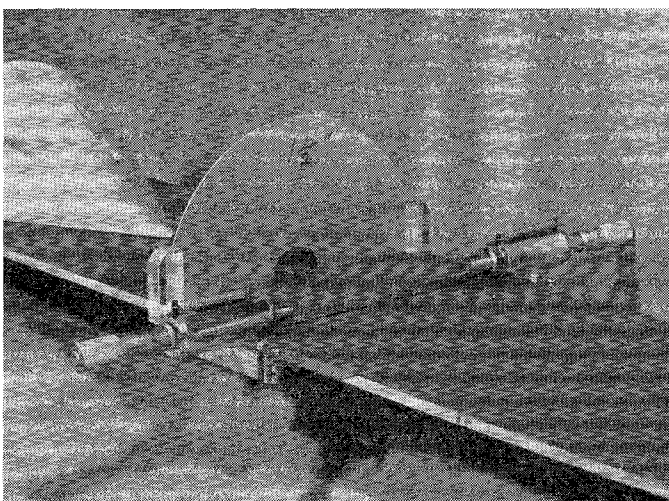


Fig. 8—Obstacles on the image line: (from right to left) adjustable matching pins; 0.20-inch unipole; 1 1/2-inch iris; and tapered matched load.

desired reflection coefficient seems to be the most efficient matching element available. However, where loss is not important, very convenient adjustable pins can be mounted on the image surface to produce any desired reflections.

#### APPENDIX

The integration of (6) yields a final expression for dielectric rod attenuation given by (7) and repeated below

$$\alpha_d = 27.3(\epsilon\phi_0/\lambda_0)R \text{ db/m.} \quad (7)$$

The ratio factor  $R$  is given as

$$R = \frac{\frac{\epsilon-1}{q^2} \frac{f^2 + \left(\frac{1}{p^2}\right) - \left(\frac{1}{p^4}\right)}{\left(\frac{1}{p^2} + \frac{1}{q^2}\right)} + (U^2 + V^2)X + \frac{4UV}{p^4}}{D} \quad (11)$$

where

$$D = UX(\epsilon + V^2) + UY(1 + V^2) + \frac{2V}{p^4}(\epsilon + U^2) - \frac{2V}{q^4}(1 + U^2)$$

$$U = \left[ \frac{\left(\frac{\epsilon}{p^2} + \frac{1}{q^2}\right)}{\left(\frac{1}{p^2} + \frac{1}{q^2}\right)} \right]^{1/2}$$

$$V = \left[ \frac{(\epsilon f + g)}{(f + g)} \right]^{1/2}$$

$$X = f^2 + \frac{(2f + 1)}{p^2} - \frac{1}{p^4}$$

$$Y = -g^2 - \frac{(2g - 1)}{q^2} + \frac{1}{q^4}.$$

Carrying out the operations indicated by (9) yields a final value of image surface loss

$$\alpha_c = 69.5(R_s/\eta\lambda_0)R' \text{ dB/m.} \quad (10)$$

The ratio factor  $R'$  turns out to be

$$R' = \frac{\frac{f(I)}{J_1^2(p)} + \frac{f(H)}{K_1^2(q)}}{\pi \left(\frac{2a}{\lambda_0}\right) \cdot D}. \quad (12)$$

Here

$$\begin{aligned} f(I) &= \frac{2}{3} \epsilon^2 \frac{S(2S + 3)}{p^3} \{I_1 + J_0(p)J_1(p)\} \\ &\quad + I_1 \frac{V^2(\epsilon - 1)}{p(p^2 + q^2)} - \frac{1}{3} I_0 \epsilon^2 \frac{(S^2 - 3)}{p^3} \\ &\quad - \frac{1}{3} \epsilon^2 \frac{S^2}{p^4} J_1^2(p) \\ f(H) &= -\frac{2}{3} \frac{T(2T + 3)}{q^3} \{H_1 + K_0(q)K_1(q)\} \\ &\quad + H_1 \frac{V^2(\epsilon - 1)}{q(p^2 + q^2)} - \frac{1}{3} H_0 \frac{(T^2 - 3)}{q^3} \\ &\quad - \frac{1}{3} \frac{T^2}{q^4} K_1^2(q). \end{aligned}$$

For the above

$$I_0 = \int_0^p J_0^2(z) dz \quad I_1 = \int_0^p J_1^2(z) dz$$

$$H_0 = \int_q^\infty K_0^2(z) dz \quad H_1 = \int_q^\infty K_1^2(z) dz$$

$$S = \left( \frac{UV}{\epsilon} - 1 \right) \quad T = (UV - 1).$$

